Ecological Indicators 148 (2023) 110124

Contents lists available at ScienceDirect

Ecological Indicators

journal homepage: www.elsevier.com/locate/ecolind

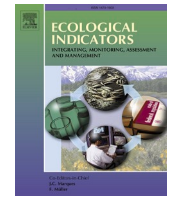

Original Articles

# Insect infestations have an impact on the quality of climate reconstructions using *Larix* ring-width chronologies from the Tibetan plateau

Sugam Aryal [a], Jussi Grießinger [a], Mohsen Arsalani [a], Wolfgang Jens-Henrik Meier [a], Pei-Li Fu [b], Ze-Xin Fan [b], Achim Bräuning [a,*]

[a] *Institute of Geography, Friedrich-Alexander-University Erlangen-Nürnberg, Wetterkeuz 15, 91058 Erlangen, Germany*
[b] *Key Laboratory of Tropical Forest Ecology, Xishuangbanna Tropical Botanical Garden, Chinese Academy of Sciences, Mengla, Yunnan 666303, China*

A R T I C L E I N F O

*Keywords:*
Yunnan
Larch budmoth
Minimum temperature
Outbreak
Defoliator
Dendrochronology

A B S T R A C T

Insect outbreaks are proven to harm trees, reducing their biomass accumulation due to the defoliation of leaves during the growing season. Various defoliators are responsible for the formation of extremely narrow tree rings in different tree species. In climate reconstructions based on tree-ring width, such narrow rings are often considered as noise, because their formation is not entirely caused by climatic conditions. Thus, the impact of defoliators should be removed (nullified) for unbiased climate reconstructions. This study mainly describes a statistical approach to disentangle the effects of Larch budmoth(LBM) (*Zeiraphera diniana*) and climate for an unbiased temperature reconstruction in the Bai-Ma mountain area in Southwest China using *Larix potaninii*. After applying our new approach, growth-climate relationships improved significantly ($p < 0.05$), especially with minimum temperature during the growing season (June-September). The resulting temperature reconstruction (BTmin) covers the period 1712–2020 CE (313 years). Our final temperature reconstruction for the Bai-Ma area showed a wiggly trend from 1712 to 1980, with some cool periods (1791–1853 and 1888–1930) and warm episodes (1724–1745, 1854–1887, 1950–1967). During the recent 50 years, BTmin reveal an alarming warming trend of up to 0.4 °C per decade. We also observed a strong coherency of BTmin with regional temperature series. Furthermore, we detected a differential effect of various climate modes, with the most substantial impact of the Atlantic Multidecadal Oscillation (AMO) on BTmin ($p < 0.01$). Interestingly, the Pacific Decadal Oscillation (PDO) showed a coupled effect along with AMO on BTmin. As revealed in this study, removing the LBM effect improved the chronology's climate sensitivity, leading to a more robust transfer function and in terms of insect infestations unbiased climate reconstructions. Thus, it is recommended to check ring-width data for any periodicity potentially related to insect outbreaks and correct the original data before using tree-ring chronologies for climate reconstruction.

## 1. Introduction

The recent global warming has affected forest growth globally by changing the mean and variability of temperature and precipitation. Precise knowledge about regional long-term climate variability is essential to correctly assess current climatic trends and to disentangle the cascading effects on regional ecological systems. There have been multiple attempts to reconstruct past climate using various proxies. Tree-ring width (TRW) has been used to reconstruct centuries or millennium-long climate variability in different parts of the world (Esper et al., 2002; Büntgen et al., 2008; Wilson et al., 2016). Due to its ability to reconstruct yearly climate variability, TRW is favored by scientists globally.

Besides climate, tree growth is also affected by several internal and external factors (Cook, 1987). For example, trees are additionally prone to biologically triggered growth trends. For non-biased climate reconstructions without such biological noise, it is essential to remove these biological growth trends using a statistical approach called standardization (Speer, 2010). Non-climatic growth trends can also be related to anthropogenic causes (such as pruning or pollarding) (Abiyu et al., 2018), but also to natural factors (such as competition and growth release) (Castagneri et al., 2022). In addition, insect outbreaks may have a strong impact on TRW-series of different tree species (Morrow and Lamarche, 1978; Jardon et al., 1994; Ryerson et al., 2003; Pohl et al.,

* Corresponding author.
*E-mail address:* achim.breauning@fau.de (A. Bräuning).

https://doi.org/10.1016/j.ecolind.2023.110124
Received 2 January 2023; Received in revised form 3 March 2023; Accepted 6 March 2023
Available online 15 March 2023

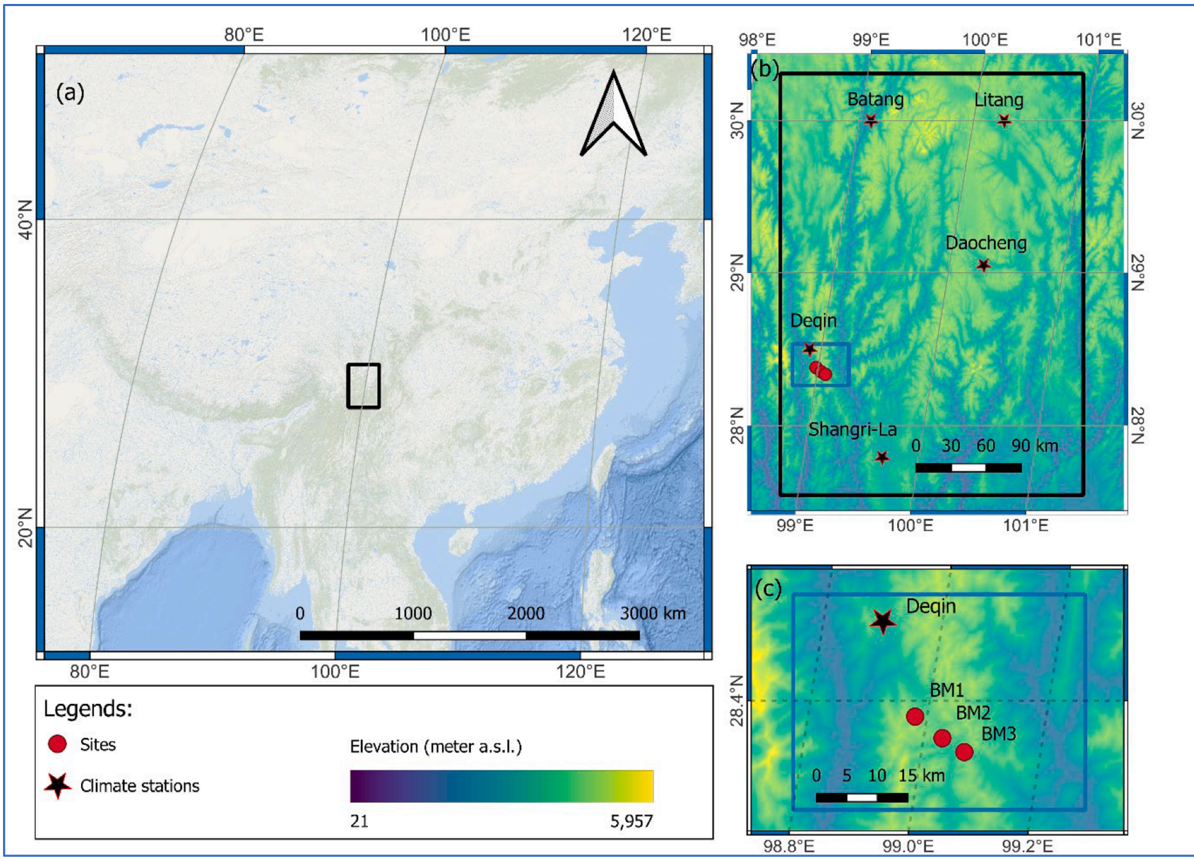


**Fig. 1.** Maps showing the location of the study area (black rectangle) in northern Yunnan inside China (a), the location of climate stations around the tree-ring sampling sites (b), and a detailed map of the study area with three study sites (BM1, BM2, BM3), and the nearest climate station (c).

2006; Fan and Bräuning, 2017), as was shown in the eastern spruce budworm (*Choristoneura fumiferana* Clem.) (Campbell et al., 2006; Fraver et al., 2007), forest tent caterpillar (*Malacosoma disstria* Hubner) (Hogg et al., 2002), larch sawfly (*Pristiphora erichsonii* Httg.) (Jardon et al., 1994; Girardin et al., 2001), and the larch budmoth (*Zeiraphera sps.*) (Fan and Bräuning, 2017; Büntgen et al., 2020). However, any periodicity in TRW series related to regular insect outbreaks is noise for analyses of climate-growth relationships, which has to be removed from TRW chronologies before climate reconstructions can be envisaged.

In China and surrounding regions, there have been studies detecting LBM outbreaks and their impact on tree growth. In 1988, LBMs (*Zeirophera lariciana* and *Zeirophera grisecana*) reduced the radial growth of *Larix principis* by 47–86% in the Saihanba forest region in Hubei province (Bi et al., 2006 as cited in Fan and Bräuning, 2017). Similarly, an outbreak of *Z. dianianai* in 2005 affected an area of 300 km$^2$ in Qinghai province, defoliating 40–90% of *L. potaninii* trees (Cao and Wang, 2006 as cited in Fan and Bräuning, 2017). In north-eastern China, Huang et al. (2010) reported a severe outbreak of caterpillar (*Dendrolimus superans* Butler) in 2003, decreasing the above-ground biomass of *L. gmelnii* by 14.62–56.84%. Most of the existing studies regarding the LBM outbreak in *Larix* were confined in the northern part of China, leaving the high-elevation area of southern China, including the Tibetan Plateau, understudied.

Mass propagation of insects often follows a cyclic pattern. The reconstruction of the larch budmoth (LBM) outbreaks in the European Alpine region revealed a regular cycle of 8–10 years (Büntgen et al., 2020). A similar frequency was also reported in northern Yunnan (Fan and Bräuning, 2017). *Larix* species, in general, have a high dendroclimatic potential due to their slow and sensitive radial growth. The frequent outbreaks of defoliators like the larch budmoth and the larch sawfly make the tree species skeptical of being used for climate reconstruction efforts. Attempts have been applied to correct affected *Larix* raw TRW chronologies for such LBM effect prior to the final climate reconstruction, e.g., by using the maximum latewood density (MXD) (Büntgen et al., 2006). Later, Büntgen et al. (2009) proposed several statistical methods to identify LBM-affected tree rings using a non-host tree species. Since then, there have been many attempts to reconstruct climate using TRW of *Larix* species. However, the possible impacts of the LBM on climate reconstruction using *Larix* were not always assessed (Fan et al., 2010; Davi et al., 2021; Jiang et al., 2021). LBM is known to have both immediate and legacy effects on tree ring and xylem anatomical features by reducing biomass accumulation, lumen area and the number of cells, resulting in the formation of narrow rings for several years (Castagneri et al., 2020). The growth depression after an LBM outbreak can result in weaker growth-climate relationships, leading to unrealistic or biased climate reconstructions (Büntgen et al., 2009; Fan and Bräuning, 2017).

In this study, we aim to reconstruct past temperature conditions at the southern margin of the Tibetan plateau (TP) using raw TRW series of *Larix* to assess the application of a new statistical method for removing periodicities in the growth series related to LBM outbreaks, while retaining climate-related growth variations.

## 2. Material and methods

### 2.1. Study area and climate

Our study includes data collected from the Bai-Ma Snow Mountain area located at the southeastern margin of the Tibetan plateau (Fig. 1). The site is under the influence of the South Asian Summer Monsoon (SASM), with maxima in temperature and precipitation occurring during the summer monsoon season (June-September). The primary moisture

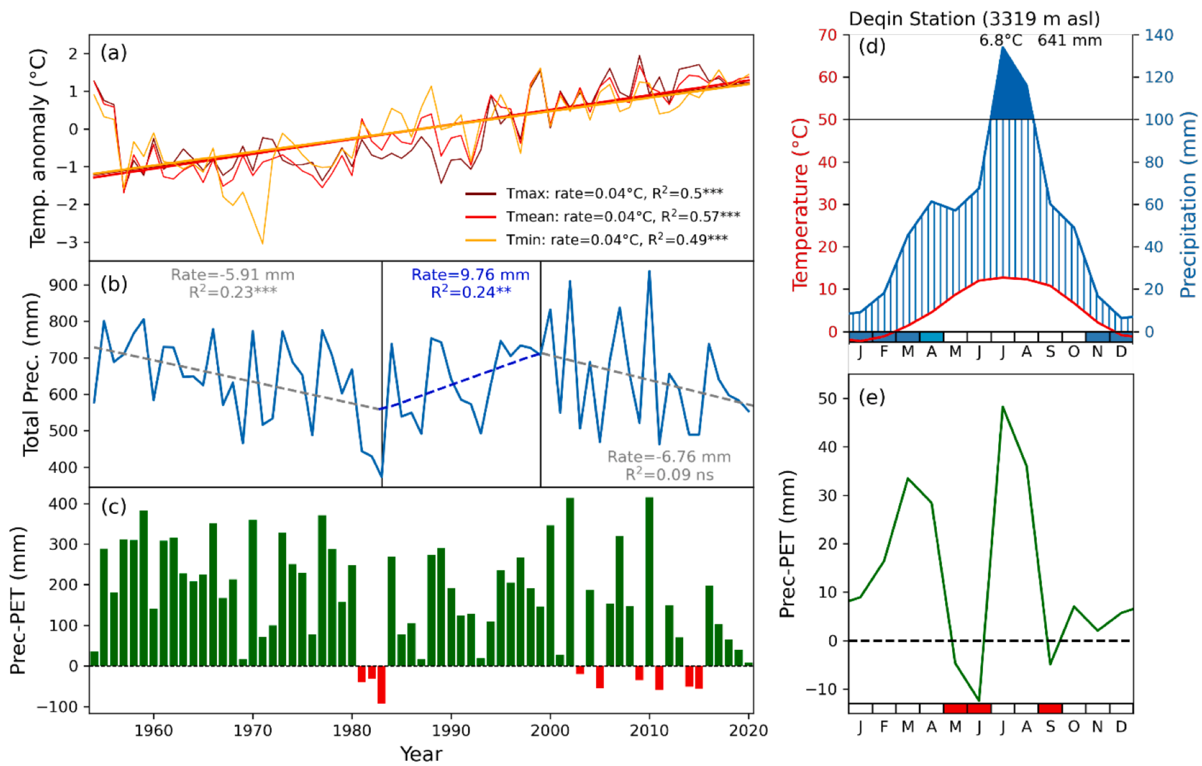


**Fig. 2.** Trends of climate parameters at the Deqin climate station: (a) anomalies of mean annual maximum, minimum and average temperature compared to 1954–2020 mean, (b) total annual precipitation, (c) total annual water balance (subtracting potential evapotranspiration from precipitation). (d) climate diagram of Deqin, including mean monthly temperature and precipitation, and (e) mean monthly water balance in Deqin. Source: National Meteorological Information Center (NMIC), China.

**Table 1**
Statistics of site-specific raw tree-ring width chronologies.

| Site | Elevation | First-year | Last-year | Cores (trees) | Mean inter-series correlation (Rbar) | Signal-noise Ratio (SNR) |
|---|---|---|---|---|---|---|
| BM1 | 4200 | 1711 | 1999 | 33 (21) | 0.59 | 12.09 |
| BM2 | 4107 | 1682 | 2020 | 30 (16) | 0.64 | 25.68 |
| BM3 | 3854 | 1800 | 2020 | 27 (16) | 0.61 | 7.76 |
| BM123 | | 1682 | 2020 | 90 (53) | 0.55 | 24.54 |

source of the study area originates from the Bay of Bengal (Xu et al., 2003).

The nearest climate station to the sampling sites is located in the county town of Deqin (3319 m asl). The maximum monthly mean (1954–2020) temperature recorded in summer (July) is 18.1 °C, whereas the minimum monthly mean temperature occurring in January is −6.5 °C (Fig. 2d). Since 1960, the study site has experienced a rapid increase in temperature of 0.04 °C per year (Fig. 2a), with long-term mean annual temperature and total annual precipitation being 6.8 °C and 641 mm, respectively. On the other hand, the total precipitation first experienced a significant decreasing trend from 1954 to 1983 (rate −5.91 mm per year) and then a significant increasing trend (rate 9.76 mm per year) until 1999 (Fig. 2b). Precipitation trend since 2000 is decreasing at an even higher rate (rate −6.76 mm per year), however, this trend is due to the shortness of the period not statistically significant ($p = 0.20$). Most of the years had a positive mean annual water balance at our study site, except for the periods 1981–1983, 2003, 2005, 2009, 2011, and 2014–2015 (Fig. 2c). The monthly water balance in May, June and September is negative, depicting that the pre-monsoon (May), early-monsoon (June), and late-monsoon (September) months experience high PET rates due to corresponding high temperatures (Fig. 2e).

## 2.2. Sample collection and preparation

Tree-ring samples were collected during two field visits in autumn 2020 and spring 2021 (BM2 and BM3) from a mixed conifer forest growing on a northeast exposed slope. Trees on the sampling site consisted of old and evenly aged *L. potaninii* trees. We aimed to collect two cores from each tree using an increment borer at breast height (1.3 m), avoiding disturbed and unhealthy trees. Besides, we also incorporated samples in our study that were collected in 2004 (BM1) within a previous study (Fan and Bräuning, 2017). Altogether, 90 tree core samples from 53 trees were used in this study (referred as site 'BM123′) (Table 1).

Tree-ring widths (TRW) were measured under a stereo-microscope and dated with the known date of formation of the outermost ring according to the sampling date. Tree-ring measurements were done using a LINTAB 5 measurement system at a resolution of 0.01 mm using TSAP software (RINNTECH Inc.). After measuring all samples, we used the alignment plot technique to crossdate the individual series by visually matching tree-ring patterns and assessing the statistical parameters Gleichläufigkeit (GLK, sign test) and t-value. The crossdating quality was checked using the computer program COFECHA (Holmes, 1983), and, if necessary, tree-ring series were corrected by inserting missing rings. The proportion of missing rings accounts for 0.143% of all measured rings. Subsequently, we applied a signal-free age-dependent spline curve-fitting approach (Melvin and Briffa, 2008) to minimize the removal of any long-term climatic variance in RCSigFree 45v2b (https://www.ldeo.columbia.edu). The chronology statistics, such as the sub-sample signal strength (SSS), mean correlation between trees (Rbar), and signal-to-noise ratio (SNR), were considered as a basis for judging the suitability for the further utility of our chronology. Hence, statistics were calculated using 'dplR' (Bunn, 2008) package based on R Software (R Development Core Team, 2021). Afterwards, the master chronology was calculated using a bi-weight robust mean from all detrended series. The oldest part of our chronology (1682– 1711 CE) had

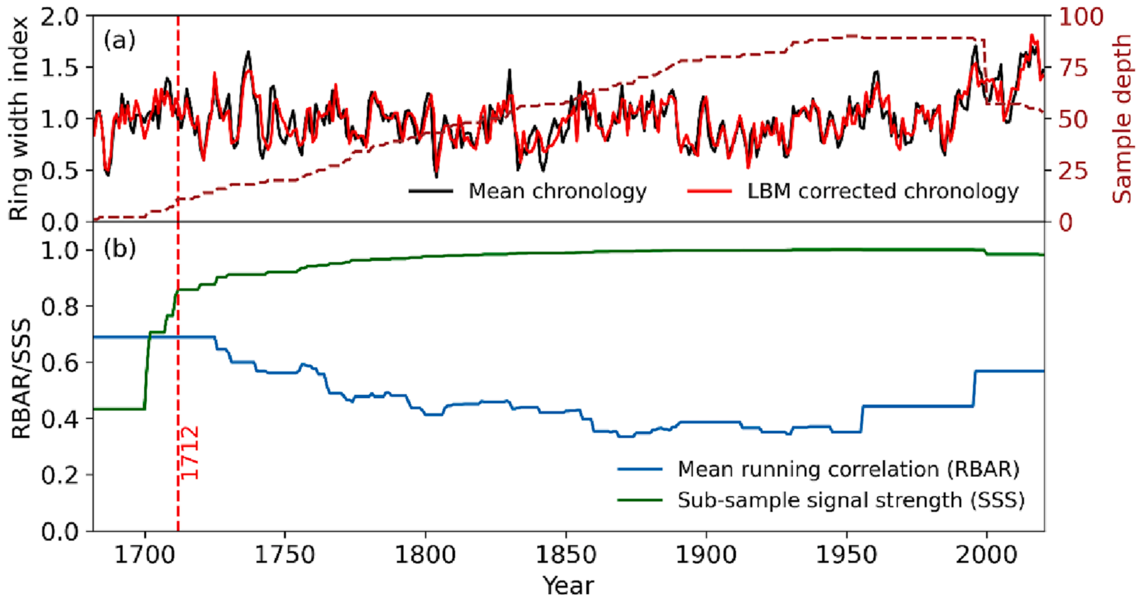


**Fig. 3.** Baima Larix (BML) mean and LBM-corrected tree-ring width index chronologies and their sample depth (a), and chronology statistics of the LBM -orrected chronology (b). The vertical dashed line marks the year 1772, after which the chronology is robust, passing the threshold of SSS > 0.85.

to be truncated at the commonly used threshold limit of SSS > 0.85 (Allan, 2017). Hence, we considered the chronology from 1712 to 2020 CE, which is reliably replicated for studying climate–growth relationships.

### 2.3. Removal of the LBM effect in the TRW series

A previous study on the same species (Fan and Bräuning, 2017) in a nearby study area detected a 7–9 year cycle of TRW depression caused by larch budmoth (LBM). Since detection of LBM was not our principle objective, we recommend to read Fan and Bräuning (2017) for more details about the historical outbreak in the site. It was highly recommended to remove or correct such non-climate-related periodic growth depressions for further high-frequency climate reconstruction. Previous research has successfully removed the LBM effect from a Larix MXD chronology to reconstruct regional temperature (Büntgen et al., 2006). Since it was not feasible to apply the same method to our standard chronology, we applied the Fast Fourier Power Transformation (FFT) technique to remove the LBM effect using the scipy module (Virtanen et al., 2020) in the Python environment. This method involves (i) extracting the power spectrum of various frequencies using the FFT method, (ii) removing the frequencies with 7 to 9 Hz, and (iii) using the inverse FFT method to obtain the final chronology free from 7 to 9 years' cyclic components. We subsequently used the Multi Taper Morlet wavelet analysis to compare the original and the LBM-adjusted chronologies (Fig. A1) using the method explained by Torrence and Compo (1998). In the next step, we compared the difference between the original raw chronology and the LBM-adjusted chronology. We observed a significant difference between the chronologies only for periods when the 7–9 year cyclicity was statistically significant (Fig. A1), advocating the removal of the LBM effect without affecting the climatic influence. In addition, the removal of LBM increased the growth-climate correlation.

### 2.4. Climate-proxy relationship and climate reconstruction

In this study, we used the precipitation and temperature data (1960–2020) of the Deqin meteorological station to calibrate the derived growth–climate models. We calculated correlation functions and seasonal correlations using the bootstrapped method to establish a relationship between tree growth and climate variables. The stability of the growth-climate relationship was tested by calculating the 35-year moving correlation for seasons and individual months. Temperature and TRW both showed a rapid surge in the correlation period. We detrended both the temperature and TRW series and analyzed the residuals to ensure that correlation was not the result of the linear trend (autocorrelation) inherent to both series. After assuring the correlation, we developed a climate reconstruction based on a linear regression model (transfer function) derived from the growth-climate relationship analysis results. We used 61 years long Deqin temperature data to calibrate and verify the linear model using the K-fold (Hastie et al., 2009) method using the sci-kit learn module (Pedregosa et al., 2011). In this study, we used five-fold verification methods that involved randomly selecting 80% of data for calibration and the remaining 20% for verification by repeating the same method five times. During the K-fold verification process, we calculated the coefficient of determination ($R^2$), variance explained (VE), root mean square error (RMSE) and mean actual error (MAE) on the verification dataset, which means five values for each statistic.

We also calculated the chronology and calibration errors (Esper et al., 2007). For the chronology error, all the standardized indices of the individual year were sampled with replacement 1000 times and two-tailed 95% confidence limits of 1000 bootstrapped means were estimated. The residual standard error of regression of the chronology against the observed June-September temperature measured the calibration error. We identified relatively cold and warm periods in our reconstructed temperature series over the whole reconstructed period (1712–2020 CE). Years exceeding the mean after filtering with a 30-year low pass smoothing spline were considered warm years, while years below the mean were regarded as cold years. We employed a running Mann-Kendall test to capture the short-term trends in the temperature series using a Python module 'pyMannkendall' (Hussain and Mahmud, 2019). We used 50 years windows to extract the slope and $R^2$ value for the statistically sound results. To compare the effect of LBM on reconstructed temperature, we used the original *Larix* chronology (before the LBM correction) to reconstruct the June-September minimum temperature. The decadal means of reconstructed temperatures before and after the LBM correction were compared, focusing mainly on the extended cool periods. Low-temperature conditions favor LBM growth, and therefore impact trees significantly (Baltensweiler, 1993). We first calculated the deviation of the temperature series from the overall

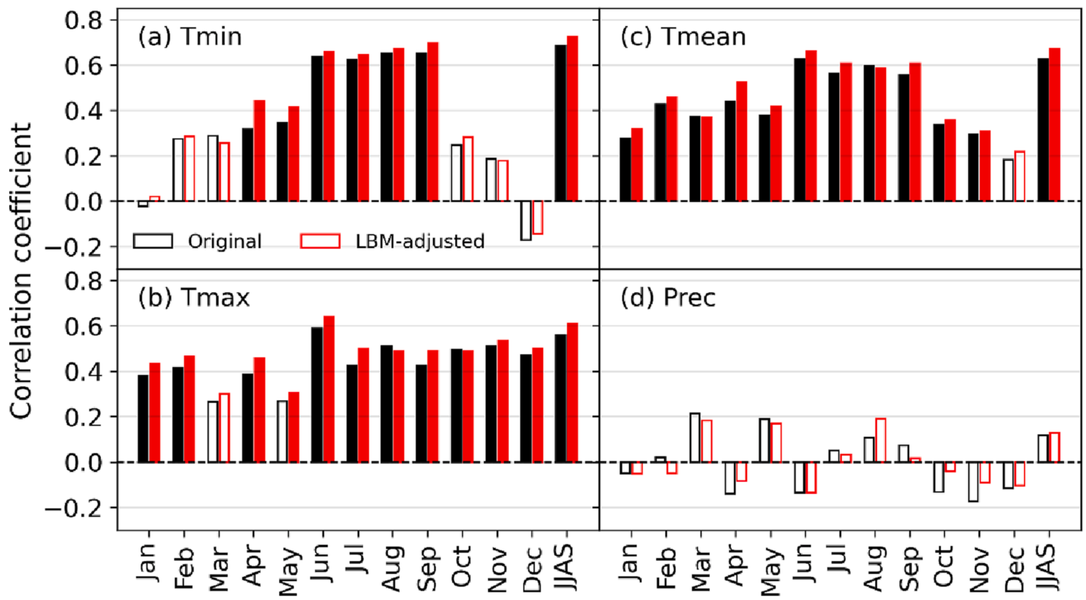


**Fig. 4.** Bootstrapped correlations between BML chronology and climate data of Deqin station. Panels a, b, c and d represent correlations with the minimum, maximum, and mean temperature and precipitation, respectively. The x-axis represents monthly windows except for JJAS, which is the period from June to September. The filled bars represent significant correlations at the 99% significance level.

(1711–2020) mean, then employed Student's *t*-test to compare the mean in moving 11-year resolution.

### 2.5. Spatial correlation and teleconnection of reconstruction

The spatial representation of our reconstructed temperature was analyzed by computing spatial correlation analyses with Climate Research Unit (CRU) gridded climate data of the reconstructed season using the KNMI-Climate Explorer (https://crudata.uea.ac.uk/cru). To extract the multi-scale decomposition, we applied the Ensemble empirical mode decomposition (EEMD) method. EEMD decomposes the signals (stationary, non-stationary or nonlinear) into a sequence of isolated intrinsic mode functions (IMFs) with various frequency domains (Wu and Huang, 2009). As suggested in previous studies, we defined four frequency domains: 3–7 year cycles as interannual, 8–34 year cycles as inter-decadal, 35–100 year cycles as multi-decadal, and >100-year cycles as centennial (Mann et al., 1995; Shi et al., 2017). Then, series of correlation analyses were performed between EEMD components and

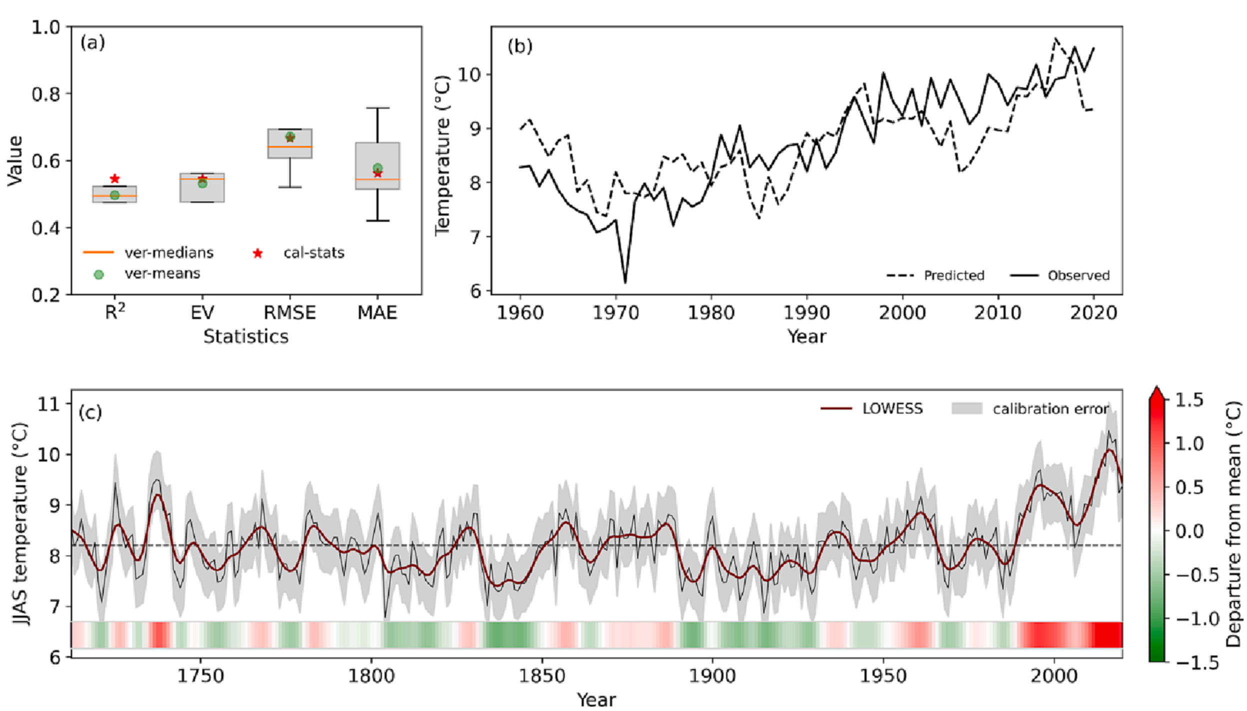


**Fig. 5.** (a) Calibration (red stars) and verification (boxplot and green dots) statistics ($R^2$: coefficient of determination, EV: Explained Variance, RMSE: Root Mean Squared Error and MAE: Mean Absolute Error) of the transfer function, (b) modelled and observed temperature and (c) June-September reconstructed temperature (black line) including the calibration error (grey band) and overall mean temperature (dashed horizontal line). (For interpretation of the references to colour in this figure legend, the reader is referred to the web version of this article.)

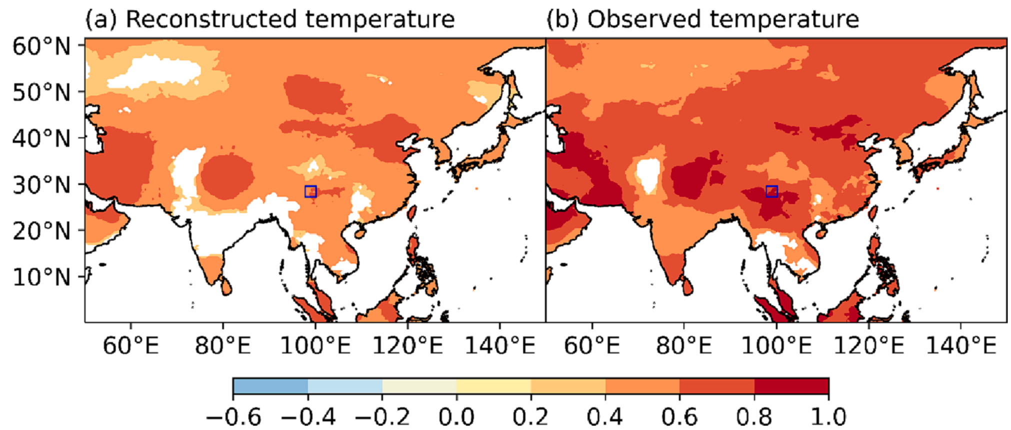


**Fig. 6.** Correlations of reconstructed JJAS minimum temperatures (a) and observed JJAS minimum temperatures (b) with CRU TS5 JJAS minimum temperatures for 1960–2020. The study site is marked by the blue square, and only significant correlations at $p < 0.01$ are shown. (For interpretation of the references to colour in this figure legend, the reader is referred to the web version of this article.)

corresponding climate modes with the same frequency domain: the inter-annual component with ENSO indices, the inter-decadal component with Pacific Decadal Oscillation (PDO), and the multi-decadal component with Atlantic Multi-decadal Oscillation (AMO). We selected the reconstructed ENSO index (Li et al., 2011), PDO index (D'Arrigo and Wilson, 2006) and AMO index (Gray et al., 2004) to analyze possible relationships with EEMD components.

## 3. Results

The final Baima Larix chronology (here after referred to as BML chronology) spans from 1683 to 2020 CE and covers 337 years. The average TRW of the trees was 0.86 ± 0.36 mm, indicating a slow-growing high-elevation environment. The individual trees included in the BML chronology showed a common growth variability over the past three centuries, with an inter-series correlation of 0.55. The majority of the samples well replicated the portion of the chronology from 1712 to 2020 CE, where the SSS value is constantly above the generally accepted threshold of SSS > 0.85. A high autocorrelation (AC1 = 0.7) of our chronology pointed to the ability of the species to record effects from the previous growing year. The long-term growth of *L. potaninii* was stable until the second half of the 20th century. After the 1970 s, the species experienced a rapid positive growth trend (Fig. 3).

The bootstrapped correlation analysis performed between our BML chronology and climate variables (Fig. 4) revealed that the growing season temperatures (maximum, minimum and mean) showed strong positive relationships with radial growth. The relationships became more robust when calculated for the whole summer monsoon season (June-September), except for Tmax, which showed the strongest correlations for the period spanning June to December. The correlation of BML chronology with Tmin (0.74, $p < 0.01$) was stronger than the correlation with Tmax (0.64, $p < 0.01$) and Tmean (0.68, $p < 0.01$). On the other hand, the BML chronology did not significantly correlate with monthly or seasonal means of precipitation. We further correlated the residuals of June-September averaged minimum temperature with the residuals of TRW. The correlation between the residuals was comparatively weaker, though still significantly positive (0.40 at $p < 0.01$) (Fig. A2).

Based on the growth-climate relationships of the BML chronology with monsoon minimum temperature, we developed a transfer function using linear regression analysis. We used the BML chronology as a predictor variable to reconstruct the minimum monsoon season temperature. The 5-fold verification showed that the average coefficient of determination ($R^2$ score) was 0.50 ± 0.17, explaining 53 ± 18 % of the variance of the observed minimum JJAS temperature. The low value of average root means square error (RMSE) (0.67 ± 0.12), and average absolute error (MAE) (0.58 ± 0.12) further corroborated the robustness of the linear model. Besides, the model calibration using the whole data (1960–2020) resulted in the final model explaining 55 % of the variance of the observed climate data. The calibration RMSE and MAE values were 0.66 and 0.56, respectively, clearly underlining the model's reliability.

The 308 years-long JJAS minimum temperature reconstruction reveals a high year-to-year variability with an overall mean of 8.3 °C (Fig. 5). Some prominent cold episodes occurred during 1746–1765, 1770–1781, 1791–1825, 1830–1853, and 1888–1930, whereas prolonged warm periods occurred in 1724–1745, 1854–1887, 1950–1967, and 1985–2020. The most extended cold period (1888–1930) experienced a −0.54 °C temperature drop, followed by a −0.43 °C drop during 1791–1825. In contrast, the most prolonged warm period (1985–2020) showed maximum warming of + 1.70 °C. The frequency of cold periods was higher before the 1950 s. After the 1950 s, and probably due to the recorded rapid increase in temperature, most of the years were observed to be warmer than the long-term average.

The reconstructed and observed JJAS minimum temperature correlated with CRUTS5 JJAS minimum temperature over a very large region (Fig. 6). Though the spatial correlations were higher for the observed temperature from Deqin station, the spatial coverage of positive correlations is well reflected by the reconstructed temperatures.

## 4. Discussion

As derived from the growth-climate relationships, it is apparent that TRW of the deciduous conifer *L. potaninii* in the Baima site was driven by temperature conditions, mainly by minimum temperature. In the high-elevation belt of Yunnan, temperatures were recognized as a growth-controlling factor by several previous studies (Liang et al., 2008; Fan et al., 2010; Liang et al., 2016). A favorable temperature is essential for the onset of tree growth. Temperature triggers the xylogenesis in conifers, influencing cambial activity and enlargement of tracheids, especially in cold and humid environments (Zhang et al., 2018). In cold climates, conifers start the xylogenesis when the daily minimum temperature reaches around 4–5 °C (Rossi et al., 2008). In contrast, the onset is governed jointly by minimum temperature and precipitation under semi-arid conditions (Ren et al., 2018). Xylem lignification generally occurs at night, when temperatures reach the daily minimum, which further explains the significance of Tmin on tree-ring formation (Hosoo et al., 2002).

The earlier part of the calibration period (1960–1999) shows a weaker yet significant correlation with Tmin during the vegetation period (JJAS), which after 1999 surged and remained stable until 2020 (Fig. A3). The possible reason for the declining seasonal (JJAS) running

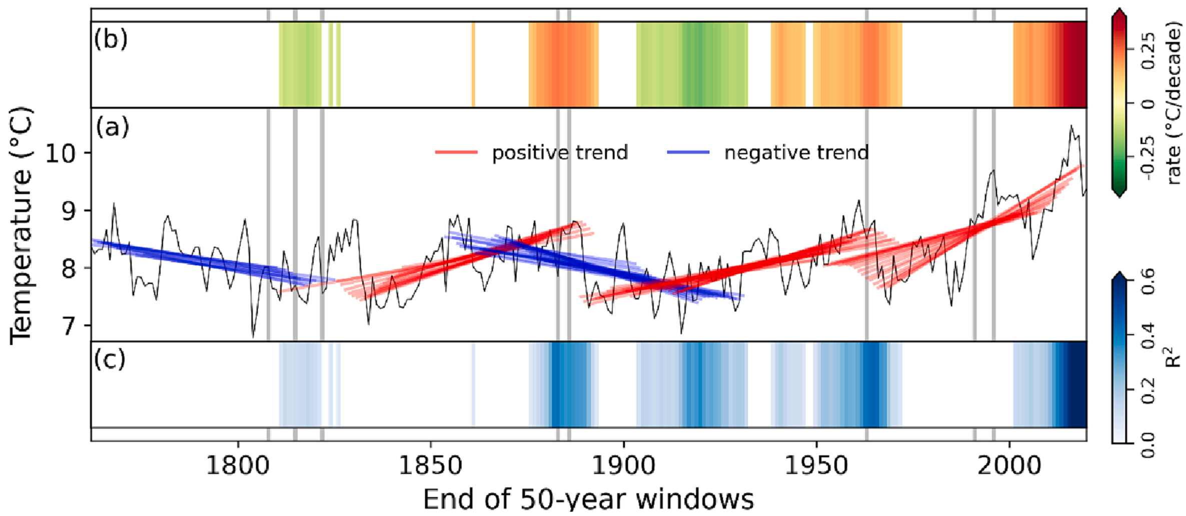


**Fig. 7.** (a) 50-year running trend analysis of reconstructed minimum summer (June to September) temperatures at Baima. The blue and red trend lines represent significant negative and positive trends., (b) slopes of the trend lines in positive/negative °C rate per decade, (c) $R^2$ values of the corresponding trend lines. (For interpretation of the references to colour in this figure legend, the reader is referred to the web version of this article.)

correlation can be a non-stationary correlation between TRW and individual months. In our study, the running correlation of June Tmin showed an insignificant correlation before 1996, which might have reduced the seasonal (JJAS) running correlation in the earlier part of the calibration. The removal of the LBM effect adjusted non-climate related growth depression, especially in 1998–2001 and 2007–2008, improving the growth-climate relationships of the chronology compared to the original chronology by 0.06. Büntgen et al. (2006) also observed enhanced growth-climate relationships of *Larix* chronologies in the European Alps after removing the LBM effect.

We compared the deviation of reconstructed temperatures before and after the LBM correction for extended cool periods between 1712 and 1950. In some cold episodes, the deviation of the reconstructed temperature before LBM correction was higher than the deviation in LBM-corrected reconstruction (Fig. A4). The more profound depression of temperature deviation of the uncorrected reconstruction indicates that the LBM-corrected chronology nullifies the impact of the outbreak. In contrast, such depression is considered a low-temperature period in the uncorrected reconstruction. The overestimation of the cold years in the uncorrected reconstruction may result from reduced biomass accumulation due to defoliation (Castagneri et al., 2020). The cold winters reduce the egg mortality of LBM and increase the diapause leading to phenological synchrony between LBM larvae and host trees, which results in a climate-independent growth reduction in subsequent growing seasons (Büntgen et al., 2020). The narrow TRW due to defoliation can result in the prediction of a falsely low-temperature year. The maximum difference between the corrected and uncorrected reconstruction in our study was within 0.25 °C (Fig. A4). LBM's effect varied with site conditions, including elevation (Peters et al., 2017; Rozenberg et al., 2020). Therefore, correcting LBM can be crucial to derive realistic climate reconstructions using Larix species, especially for areas, where severe effects of LBM may occur. Previous research has shown a coupled effect of drought and defoliation in some conifer species (e.g. Jacquet et al., 2014; Bouzidi et al., 2019). However, in our site, the tree ring chronology did not show any significant relationship with moisture conditions (Fig. 4d). As shown in the climate graph (Fig. 2c), it is clear that our site is not prone to severe drought conditions. Besides, *L. potaninii* is a deciduous tree growing at an elevation of about 4000 m asl, with an actual growing season from mid-April to September coinciding with the peak of the South Asian Summer Monsoon (SASM). Therefore, the insect-related defoliation of leaves occurs during the highly wet summer monsoon season.

The reconstructed Baima JJAS minimum temperature (BTmin) showed various cool and warm periods during the past 308 years (Fig. 5c). Some apparent cold events overlap with large and well-known volcanic eruptions (Briffa et al., 1998), severely affecting the global climate. We tested the impact of volcanic eruptions using a superposed epoch analysis (Lough and Fritts, 1987), but found that the effect of volcanic eruptions on BTmin was insignificant. Depending on the seasonal timing of the respective volcanic event, some eruptions affected tree growth in the event year. In contrast, others triggered growth depressions in the years following the event (legacy effect) (Fig. not shown). The impact of volcanic eruptions on a tree-ring series also depends on the geographical location, seasonality, composition of volcanic aerosols, and large-scale atmospheric circulation (Jones et al., 1995; Robock and Mao, 1995; Anchukaitis et al., 2010). Overall, BTmin showed an increasing trend. However, when analyzing 50-year running windows, various increasing and decreasing trends became apparent (Fig. 7). We identified significant decreasing trends from 1761 to 1826, followed by increasing trends from 1826 to 1893. Afterwards, the BTmin experienced decreasing trends before the rapid increase after 1900. The increment rate after 1900 surged dramatically from 0.10 °C to 0.42 °C per decade. Although the present rise in temperature has a positive effect on the growth of *Larix* in the study area, the future impact of such a drastic temperature trend might not be favorable. Studies conducted in the Hengduan mountains on the southern declivity of the TP have shown that the treeline positions have not significantly changed since 2000. However, the relative vegetation coverage has significantly increased at the treeline margin (Zou et al., 2022). The increase in temperature generally accompanies an increase in potential evapotranspiration (Thornthwaite, 1948), resulting in drier soil and atmospheric conditions, ultimately hindering plant growth (Körner, 2015). Studies in the European Alps have shown decreased radial growth in warmer and drier low-elevation sites compared to high-elevation sites, ultimately causing an upward shift in species range (Obojes et al., 2018). A similar elevation-dependent growth trend was also reported on *L. gmelinii* in northern China (Bai et al., 2019). The decreasing growth trend in lower elevations advocates for the possible adverse effect of rapid temperature increase in high elevation sites in the future. Further, in Chinese mountain regions, *Larix*'s species range is likely to shift and extend towards the north (Song et al., 2004) or to decrease (Li et al., 2006) in future climate scenarios. A study by Mamet et al. (2019) reported an upward shifting treeline of *L. potaninii* in China. A continuous range shift may result in species extinction for species growing in high elevation areas.

We compared our reconstruction (BTmin) with other summer

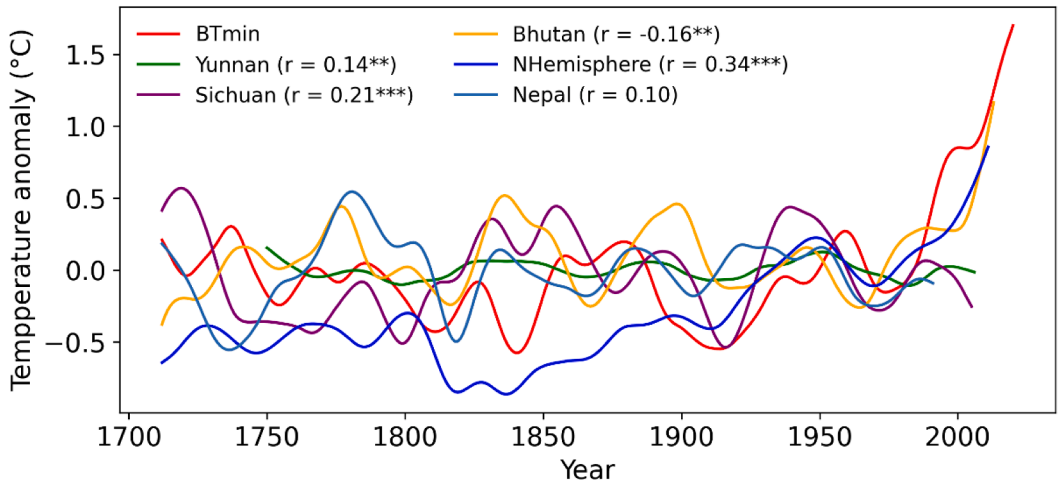


**Fig. 8.** Comparison of 30-year low pass filter of BTmin with 30-year low pass filter of other summer temperature reconstructions from Yunnan, Sichuan, Bhutan, Nepal and the Northern hemisphere. The "r" notation inside the parentheses represents Pearson's correlation of the corresponding reconstruction with BTmin. "***" and "**"represent significance at $p < 0.01$ and $p < 0.05$, respectively.

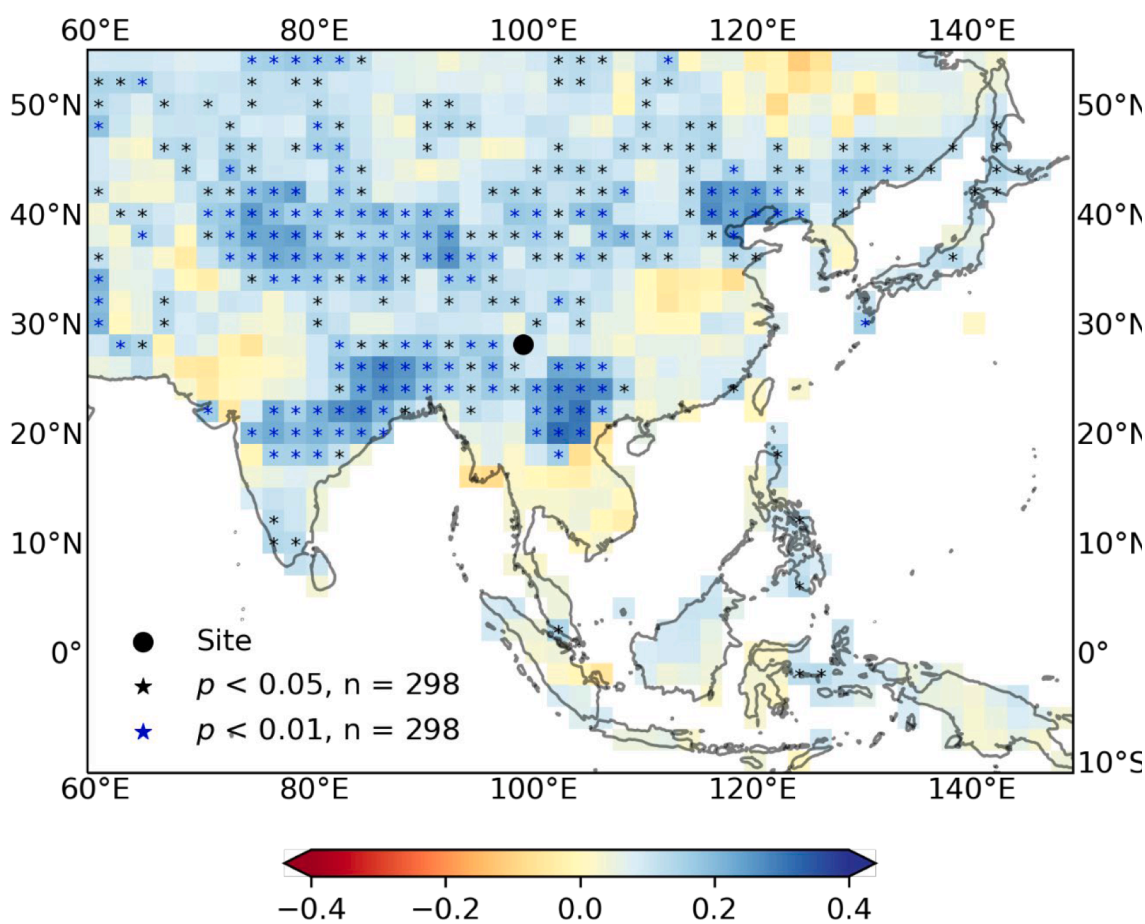


**Fig. 9.** Pearson's correlation between the BTmin and PAGES Asia2k gridded summer temperature reconstruction. The grids with blue and black asterisks represent significant correlations at $p < 0.01$ and $p < 0.05$, respectively. (For interpretation of the references to colour in this figure legend, the reader is referred to the web version of this article.)

temperature reconstructions from Yunnan (Fan et al., 2009), Sichuan (Zhang et al., 2022), Bhutan (Krusic et al., 2015), Nepal (Cook et al., 2003), and the Northern hemisphere (Wilson et al., 2016) (Fig. 8). The significant positive correlation of our BTmin with reconstructions from Yunnan, Sichuan and the northern hemisphere underlines the validity of our reconstruction. The correlation, however, was negative or insignificant with reconstructions from Bhutan and Nepal. There can be several reasons for such heterogeneity between reconstructions in complex mountain topography, such as the location and elevation of the sites and the tree species used for the reconstruction (species-specific response). When compared with PAGES Asia2k gridded summer temperature reconstruction (Cook et al., 2013), our BTmin showed a good

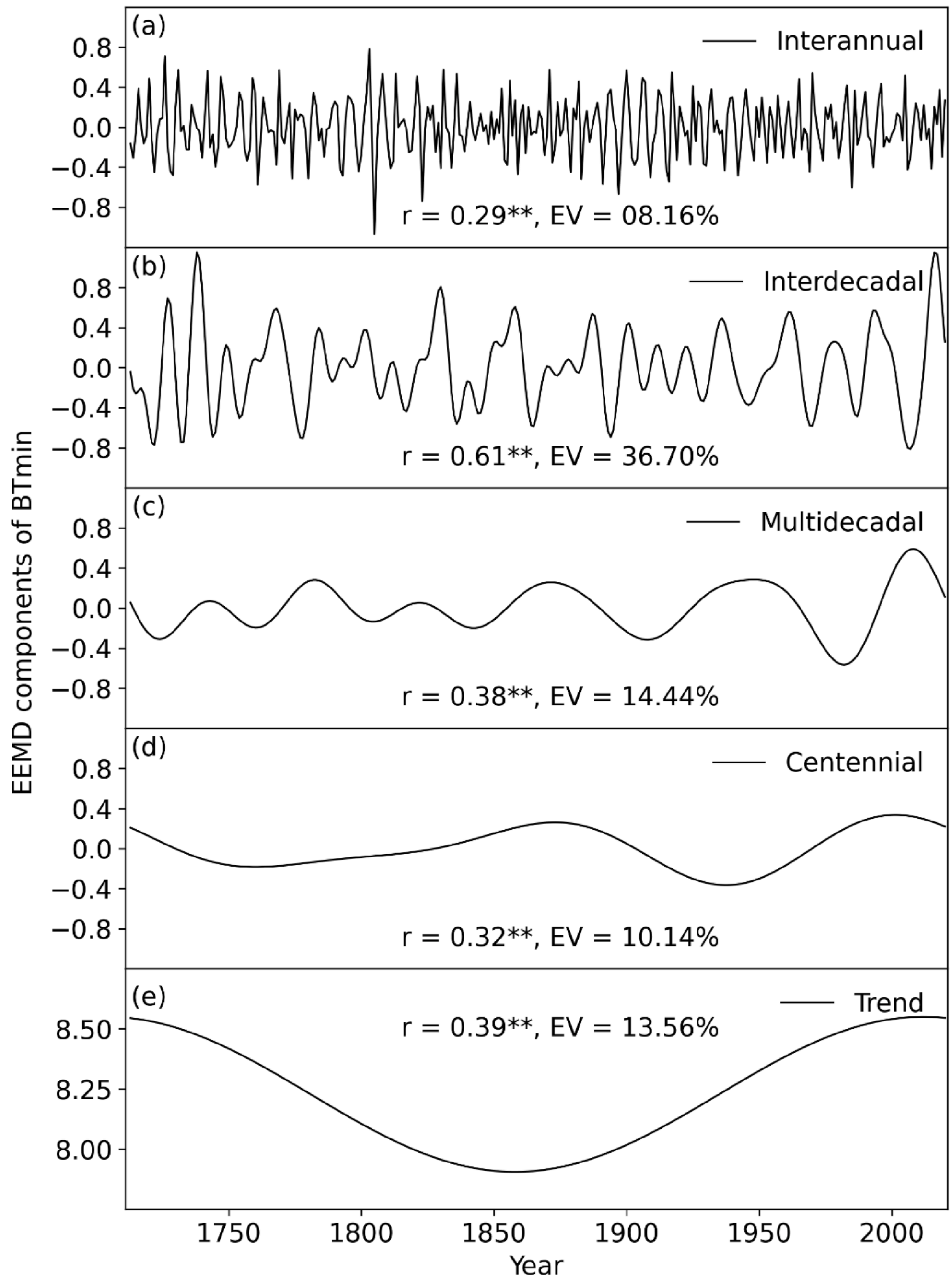


**Fig. 10.** (a)-(e) Extracted frequency components of the BTmin temperature reconstruction using ensemble empirical mode decomposition. r: correlation with the BTmin, EV: explained variance, and **: significant correlation at $p < 0.01$.

representation of regional temperature in most high-elevation areas and high-latitude Asia (Fig. 9).

Fig. 10 represents the different Ensemble empirical mode decomposition (EEMD) components of reconstructed temperature (BTmin). The inter-annual component (Fig. 10a) explains 8.16% of the total variance of BTmin. The overall and running correlation of the inter-annual component with the ENSO index was not statistically significant (Fig. 11a). This clarifies the absence of direct effect related to ENSO events in our study site. The insignificant effect of ENSO was also observed in the regional minimum temperature reconstructed using a network of multi-species chronologies in Yunnan province (Keyimu et al., 2021). The overall correlation of the very strong inter-decadal component (36.70% of the variance, Fig. 10b) with PDO was statistically insignificant ($r = -0.10$; $p > 0.1$), showing a negative effect of PDO on BTmin. However, the strength of this correlation varied over time. The correlation with PDO was statistically significant during the 1870 s and 1920 s (Fig. 11b). The multi-decadal component (Fig. 10d) strongly followed the AMO pattern with a correlation of $r = 0.51$ ($p < 0.01$) (Fig. 11c). Previous studies in southwest China also reported a positive relationship between AMO and reconstructed temperature (Keyimu et al., 2021; Zhang et al., 2022). In southeast and east Asia, a positive AMO mode extends the duration of the summer monsoon (Lu et al., 2006). In addition, the temperature anomalies in East Asia lead to the occurrence of the positive AMO phase, resulting in a positive relationship between temperature and AMO (Li et al., 2015). The effect of global circulation patterns on the local or regional climate follows complex pathways. In some regions, two or more climate modes interact and exert a coupled (and mixed) effect on the regional climate (Dong, 2016;

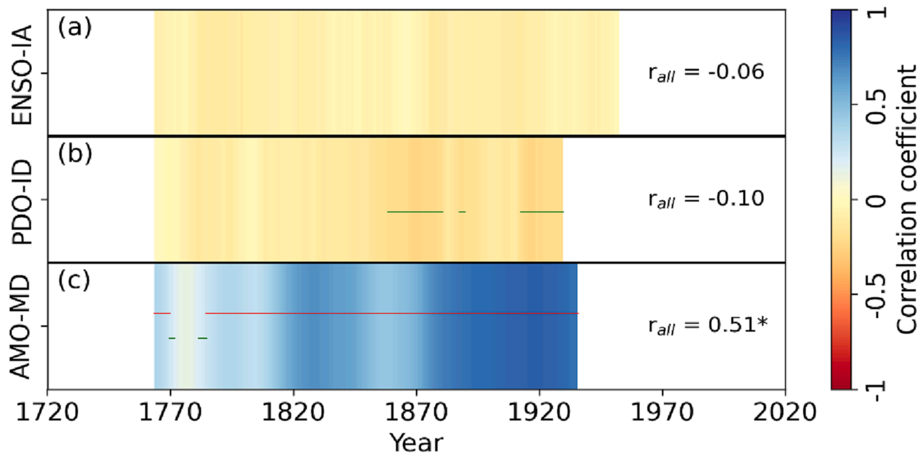


**Fig. 11.** 101-year running correlation between (a) ENSO and inter-annual component (IA), (b) PDO and inter-decadal component (ID) and (c) AMO and multi-decadal component (MD) of BTmin. The years along the y-axis represent the centers of 101-year windows. '$r_{all}$' is the overall correlation. The red line represents $p < 0.01$, and the green line represents $p < 0.05$. (For interpretation of the references to colour in this figure legend, the reader is referred to the web version of this article.)

Wu and Mao, 2017). For a detailed examination of the unstable relationship between PDO and the inter-decadal component of BTmin, we further inspected any possible coupled effect of PDO and AMO on BTmin. We found that BTmin was more sensitive to PDO in phases when PDO and AMO were negatively correlated. That means a positive temperature anomaly was observed during positive AMO (AMO + ) and negative PDO (PDO-) phases and vice versa (Fig. A5). From Fig. A6, it is apparent that some of the prominent divergences between PDO and AMO occurred during 1790–1850 and 1904–1980, resulting in a significant correlation between PDO and the inter-decadal component of BTmin (Fig. 11b). Such a coupled effect of PDO and AMO on global temperature variability was also reported by (Maruyama, 2019).

The centennial component of EEMD explained 10.14% of the total temperature variance (Fig. 10d), which could be related to long-term solar cycles such as the Gleissberg or Suess-DeVries cycle (Peek, 2018). In the Tibetan plateau and surrounding areas, centennial and multi-centennial temperature variations are influenced by the solar cycle (Duan and Zhang, 2014; Keyimu et al., 2021; Zhang et al., 2022). In this study, the reconstruction length of roughly three centuries is not long enough for a statistically sound comparison with the centennial scale of the solar cycle. The residuals of the BTmin (Fig. 10e) followed a concave parabolic trend reaching a minimum during the 1860 s, possibly reflecting the temperature depression during the 19th century, potentially related to the 'Little Ice Age' (Yang et al., 2009; Rowan, 2017). In the southeastern TP, a TRW chronology of *L. griffithii* showed evidence of glacier advance from the end of the eighteenth to the beginning of the nineteenth century and from 1860 to 1880 (Bräuning, 2006).

## 5. Conclusions and recommendations

In this study, we proposed a statistical method to remove the effect of Larch budmoth (LBM) in *Larix potaninii* tree-ring width series before using them for climate reconstruction. This method of LBM removal resulted in an enhanced growth-climate relationship, pointing towards a more robust climate reconstruction. In our study site, the growth of Larix was strongly controlled by temperatures (minimum, mean, and maximum), with the strongest positive relationship with summer (June to September) minimum temperature. Based on this growth-climate relationship, we used the LBM-corrected chronology to reconstruct the summer season minimum temperature. The reconstructed minimum temperature showed strong consistency with regional and global temperature patterns with the differential effect of major tropical volcanic events. Our reconstruction showed an alarming rate of regional temperature increase after the 1980 s. As reported by previous studies, our reconstruction was also found to be strongly influenced by global circulation modes, with the strongest positive coherency with the Atlantic multi-decadal oscillation (AMO).

As demonstrated in this study, the removal of the LBM effect from the chronology improved climate sensitivity. Increased climate sensitivity leads to a robust transfer function and ultimately leads to unbiased and robust climate reconstructions. Based on our findings, we highly recommend checking for any periodicity related to the insect outbreak and correcting it before using tree-ring chronologies for further climate reconstruction.

## Declaration of Competing Interest

The authors declare that they have no known competing financial interests or personal relationships that could have appeared to influence the work reported in this paper.

## Data availability

Data will be made available on request.

*Acknowledgements*

We express deep gratitude to the National Meteorological Information Center (NMIC), China, for the availability of climate data. This result represents an objective of a collaborative project, YunForest. We want to thank our funding agencies, Deutsche Forschungsgemeinschaft (DFG) and the National Natural Science Foundation of China (NSFC), for funding this research. We also thank the technical staff and students of FAU and XTBG for providing immense support during field and lab work.

*Funding*

This work was supported by the Deutsche Forschungsgemeinschaft (DFG) [grant numbers BR 1895/30-1, GR 3799/4-1] and the Chinese Academy of Science.

## Appendix A. Supplementary data

Supplementary data to this article can be found online at https://doi.org/10.1016/j.ecolind.2023.110124.

## References

Abiyu, A., Mokria, M., Gebrekirstos, A., Bräuning, A., 2018. Tree-ring record in Ethiopian church forests reveals successive generation differences in growth rates and disturbance events. Forest Ecol. Manag. 409, 835–844. https://doi.org/10.1016/j.foreco.2017.12.015.

Allan, B., 2017. A comment on the expressed population signal. Dendrochronologia 44, 130–132. https://doi.org/10.1016/j.dendro.2017.03.005.

Anchukaitis, K.J., Buckley, B.M., Cook, E.R., Cook, B.I., D'Arrigo, R.D., Ammann, C.M., 2010. Influence of volcanic eruptions on the climate of the Asian monsoon region. Geophys. Res. Lett. 37 (22), n/a–n/a.

Bai, X., Zhang, X., Li, J., Duan, X., Jin, Y., Chen, Z., 2019. Altitudinal disparity in growth of Dahurian larch (*Larix gmelinii* Rupr.) in response to recent climate change in northeast China. Sci. Total Environ. 670, 466–477. https://doi.org/10.1016/j.scitotenv.2019.03.232.

Baltensweiler, W., 1993. Why the larch bud-moth cycle collapsed in the subalpine larch-cembran pine forests in the year 1990 for the first time since 1850. Oecologia 94 (1), 62–66. https://doi.org/10.1007/BF00317302.

Bi, H.M., Zhang, H., Pan, X.H., Zhu, X.Q., 2006. The effect of Zeiraphera lariciana and Zeiraphera lariciana on growth of larch plantations. Hebei J. For. Orchard Res. 21 (1), 81–82. https://www.scopus.com/inward/record.uri?eid=2-s2.0-85006840979&partnerID=40&md5=d0306f25f88a5cada3021974eef4902b.

Bouzidi, H.A., Balducci, L., Mackay, J., Deslauriers, A., 2019. Interactive effects of defoliation and water deficit on growth, water status, and mortality of black spruce (Picea mariana (Mill.) B.S.P.). Annals of Forest Science 76 (1). https://doi.org/10.1007/s13595-019-0809-z.

Bräuning, A., 2006. Tree-ring evidence of 'Little Ice Age' glacier advances in southern Tibet. The Holocene 16 (3), 369–380. https://doi.org/10.1191/0959683606hl922rp.

Briffa, K.R., Jones, P.D., Schweingruber, F.H., Osborn, T.J., 1998. Influence of volcanic eruptions on Northern Hemisphere summer temperature over the past 600 years. Nature 393, 450–455. https://doi.org/10.1038/30943.

Bunn, A.G., 2008. A dendrochronology program library in R (dplR). Dendrochronologia 26 (2), 115–124. https://doi.org/10.1016/j.dendro.2008.01.002.

Büntgen, U., Frank, D.C., Nievergelt, D., Esper, J., 2006. Summer Temperature Variations in the European Alps, a.d. 755–2004. J. Climate 19 (21), 5606–5623. https://doi.org/10.1175/JCLI3917.1.

Büntgen, U., Frank, D., Grudd, H., Esper, J., 2008. Long-term summer temperature variations in the Pyrenees. Clim. Dyn. 31, 615–631. https://doi.org/10.1007/s00382-008-0390-x.

Büntgen, U., Frank, D., Liebhold, A., Johnson, D., Carrer, M., Urbinati, C., Grabner, M., Nicolussi, K., Levanic, T., Esper, J., 2009. Three centuries of insect outbreaks across the European Alps. New Phytol. 182 (4), 929–941. https://doi.org/10.1111/j.1469-8137.2009.02825.x.

Büntgen, U., Liebhold, A., Nievergelt, D., Wermelinger, B., Roques, A., Reinig, F., Krusic, P.J., Piermattei, A., Egli, S., Cherubini, P., Esper, J., 2020. Return of the moth: rethinking the effect of climate on insect outbreaks. Oecologia 192 (2), 543–552. https://doi.org/10.1007/s00442-019-04585-9.

Campbell, R., Smith, D.J., Arsenault, A., 2006. Multicentury history of western spruce budworm outbreaks in interior Douglas-fir forests near Kamloops. British Columbia. Can. J. For. Res. 36 (7), 1758–1769. https://doi.org/10.1139/x06-069.

Cao, J.Q., Wang, K.B., 2006. Study on control Zeiraphera diniana of Larix potaninii in Kakehe forest region. Sci. Tech. Qinghai Agr. For. 2, 30–36. https://www.scopus.com/inward/record.uri?eid=2-s2.0-85006941551&partnerID=40&md5=b06312790db804d3fd20ecda46e30a1d.

Castagneri, D., Prendin, A.L., Peters, R.L., Carrer, M., Arx, G.v., Fonti, P.,, 2020. Long-Term Impacts of Defoliator Outbreaks on Larch Xylem Structure and Tree-Ring Biomass. Front. Plant Sci. 11, 1–10. https://doi.org/10.3389/fpls.2020.01078.

Castagneri, D., Vacchiano, G., Hacket-Pain, A., DeRose, R.J., Klein, T., Bottero, A., 2022. Meta-analysis Reveals Different Competition Effects on Tree Growth Resistance and Resilience to Drought. Ecosystems 25 (1), 30–43. https://doi.org/10.1007/s10021-021-00638-4.

Cook, E.R., 1987. The Decomposition of Tree-Ring Series for Environmental Studies. Tree-Ring Bulletin 47, 37–59. http://hdl.handle.net/10150/261788.

Cook, E.R., Krusic, P.J., Jones, P.D., 2003. Dendroclimatic Signals in Long Tree-Ring Chronologies from the Himalayas of Nepal. Int. J. Climatol. 23, 26–29. https://doi.org/10.1002/joc.911.

Cook, E.R., Krusic, P.J., Anchukaitis, K.J., Buckley, B.M., Nakatsuka, T., Sano, M., 2013. Tree-ring reconstructed summer temperature anomalies for temperate East Asia since 800 C.E. Clim. Dyn. 41 (11–12), 2957–2972. https://doi.org/10.1007/s00382-012-1611-x.

D'Arrigo, R., Wilson, R., 2006. On the Asian expression of the PDO. Int. J. Climatol. 26 (12), 1607–1617. https://doi.org/10.1002/joc.1326.

Davi, N.K., Rao, M.P., Wilson, R., Andreu-Hayles, L., Oelkers, R., D'Arrigo, R., Nachin, B., Buckley, B., Pederson, N., Leland, C., Suran, B., 2021. Accelerated Recent Warming and Temperature Variability Over the Past Eight Centuries in the Central Asian Altai From Blue Intensity in Tree Rings. Geophys. Res. Lett. 48 (16) https://doi.org/10.1029/2021GL092933.

Dong, X., 2016. Influences of the Pacific Decadal Oscillation on the East Asian Summer Monsoon in non-ENSO years. Atmos. Sci. Lett. 17 (1), 115–120. https://doi.org/10.1002/asl.634.

Duan, J., Zhang, Q.-B., 2014. A 449 year warm season temperature reconstruction in the southeastern Tibetan Plateau and its relation to solar activity. J. Geophys. Res. Atmos. 119 (20), 11578–11592. https://doi.org/10.1002/2014JD022422.

Esper, J., Schweingruber, F.H., Winiger, M., 2002. 1300 years of climatic history for Western Central Asia inferred from tree-rings. The Holocene 12 (3), 267–277. https://doi.org/10.1191/0959683602hl543rp.

Esper, J., Frank, D., Büntgen, U., Verstege, A., Luterbacher, J., Xoplaki, E., 2007. Long-term drought severity variations in Morocco. Geophys. Res. Lett. 34 (17), 2929. https://doi.org/10.1029/2007GL030844.

Fan, Z.-X., Bräuning, A., Yang, B., Cao, K.-F., 2009. Tree ring density-based summer temperature reconstruction for the central Hengduan Mountains in southern China. Glob. Planet. Change 65 (1–2), 1–11. https://doi.org/10.1016/j.gloplacha.2008.10.001.

Fan, Z.-X., Bräuning, A., 2017. Tree-ring evidence for the historical cyclic defoliator outbreaks on *Larix potaninii* in the central Hengduan Mountains, SW China. Ecol. Indic. 74, 160–171. https://doi.org/10.1016/j.ecolind.2016.11.026.

Fan, Z.-X., Bräuning, A., Tian, Q.-H., Yang, B., Cao, K.-F., 2010. Tree ring recorded May–August temperature variations since A.D. 1585 in the Gaoligong Mountains, southeastern Tibetan Plateau. Palaeogeogr. Palaeoclimatol. Palaeoecol. 296 (1–2), 94–102. https://doi.org/10.1016/j.palaeo.2010.06.017.

Fraver, S., Seymour, R.S., Speer, J.H., White, A.S., 2007. Dendrochronological reconstruction of spruce budworm outbreaks in northern Maine. USA. Can. J. For. Res. 37 (3), 523–529. https://doi.org/10.1139/X06-251.

Girardin, M.-P., Tardif, J., Bergeron, Y., 2001. Radial growth analysis of *Larix laricina* from the Lake Duparquet area, Québec, in relation to climate and larch sawfly outbreaks. Écoscience 8 (1), 127–138. https://doi.org/10.1080/11956860.2001.11682638.

Gray, S.T., Graumlich, L.J., Betancourt, J.L., Pederson, G.T., 2004. A tree-ring based reconstruction of the Atlantic Multidecadal Oscillation since 1567 A.D. Geophys. Res. Lett. 31 (12). https://doi.org/10.1029/2004GL019932.

Hastie, T., Tibshirani, R., Friedman, J.H., 2009. The elements of statistical learning. Data mining, inference, and prediction, 2nd ed. Springer, New York. https://doi.org/10.1007/978-0-387-84858-7.

Hogg, E.H., Brandt, J.P., Kochtubajda, B., 2002. Growth and dieback of aspen forests in northwestern Alberta, Canada, in relation to climate and insects. Can. J. For. Res. 32 (5), 823–832. https://doi.org/10.1139/x01-152.

Holmes, R.L., 1983. Computer-Assisted Quality Control in Tree-Ring Dating and Measurement. Tree-Ring Bulletin 43, 69–78. http://hdl.handle.net/10150/261223.

Hosoo, Y., Yoshida, M., Imai, T., Okuyama, T., 2002. Diurnal difference in the amount of immunogold-labeled glucomannans detected with field emission scanning electron microscopy at the innermost surface of developing secondary walls of differentiating conifer tracheids. Planta 215 (6), 1006–1012. https://doi.org/10.1007/s00425-002-0824-3.

Huang, L., Ning, Z., Zhang, X., 2010. Impacts of caterpillar disturbance on forest net primary production estimation in China. Ecological Indicators 10 (6), 1144–1151. https://doi.org/10.1016/j.ecolind.2010.03.015.

Hussain, M., Mahmud, I., 2019. pyMannKendall: a python package for non parametric Mann Kendall family of trend tests. J. open source softw. 4 (39), 1556. https://doi.org/10.21105/joss.01556.

Jacquet, J.-S., Bosc, A., O'Grady, A., Jactel, H., 2014. Combined effects of defoliation and water stress on pine growth and non-structural carbohydrates. Tree Physiol 34 (4), 367–376. https://doi.org/10.1093/treephys/tpu018.

Jardon, Y., Filion, L., Cloutier, C., 1994. Tree-ring evidence for endemicity of the larch sawfly in North America. Can. J. For. Res. 24 (4), 742–747. https://doi.org/10.1139/x94-098.

Jiang, Y., Liu, C., Zhang, J., Han, S., Coombs, C.E.O., Wang, X., Wang, J., Hao, L., Dong, S., 2021. Tree ring width-based January–March mean minimum temperature reconstruction from *Larix gmelinii* in the Greater Khingan Mountains, China since AD 1765. Int. J. Climatol. 41 (S1), E842-E854. https://doi.org/10.1002/joc.6733. https://rmets.onlinelibrary.wiley.com/doi/10.1002/joc.6733.

Jones, P.D., Briffa, K.R., Schweingruber, F.H., 1995. Tree-ring evidence of the widespread effects of explosive volcanic eruptions. Geophys. Res. Lett. 22 (11), 1333–1336. https://doi.org/10.1029/94GL03113.

Keyimu, M., Li, Z., Liu, G., Fu, B., Fan, Z., Wang, X., Wu, X., Zhang, Y., Halik, U., 2021. Tree-ring based minimum temperature reconstruction on the southeastern Tibetan Plateau. Quaternary Sci. Rev. 251, 106712 https://doi.org/10.1016/j.quascirev.2020.106712.

Körner, C., 2015. Paradigm shift in plant growth control. Curr. Opin. Plant Biol. 25, 107–114. https://doi.org/10.1016/j.pbi.2015.05.003.

Krusic, P.J., Cook, E.R., Dukpa, D., Putnam, A.E., Rupper, S., Schaefer, J., 2015. Six hundred thirty-eight years of summer temperature variability over the Bhutanese Himalaya. Geophys. Res. Lett. 42 (8), 2988–2994. https://doi.org/10.1002/2015GL063566.

Li, S., Jing, Y., Luo, F., 2015. The potential connection between China surface air temperature and the Atlantic Multidecadal Oscillation (AMO) in the Pre-industrial Period. Sci. China Earth Sci. 58 (10), 1814–1826. https://doi.org/10.1007/s11430-015-5091-9.

Li, J., Xie, S.-P., Cook, E.R., Huang, G., D'Arrigo, R., Liu, F., Ma, J., Zheng, X.-T., 2011. Interdecadal modulation of El Niño amplitude during the past millennium. Nat. Clim. Chang. 1 (2), 114–118. https://doi.org/10.1038/nclimate1086.

Li, F., Zhou, G., Cao, M., 2006. Responses of *Larix gmelinii* geographical distribution to future climate change: a simulation study. J. Appl. Ecol. 17 (12), 2255–2260. https://europepmc.org/article/med/17330460.

Liang, H., Lyu, L., Wahab, M., 2016. A 382-year reconstruction of August mean minimum temperature from tree-ring maximum latewood density on the southeastern Tibetan Plateau, China. Dendrochronologia 37, 1–8. https://doi.org/10.1016/j.dendro.2015.11.001.

Liang, E., Shao, X., Qin, N., 2008. Tree-ring based summer temperature reconstruction for the source region of the Yangtze River on the Tibetan Plateau. Glob. Planet. Change 61 (3–4), 313–320. https://doi.org/10.1016/j.gloplacha.2007.10.008.

Lough, J.M., Fritts, H.C., 1987. An assessment of the possible effects of volcanic eruptions on North American climate using tree-ring data, 1602 to 1900 A.D. Clim. Change 10 (3), 219–239. https://doi.org/10.1007/BF00143903.

Lu, R., Dong, B., Ding, H., 2006. Impact of the Atlantic Multidecadal Oscillation on the Asian summer monsoon. Geophys. Res. Lett. 33 (24), L08705. https://doi.org/10.1029/2006GL027655.

Mamet, S.D., Brown, C.D., Trant, A.J., Laroque, C.P., 2019. Shifting global *Larix* distributions: Northern expansion and southern retraction as species respond to changing climate. J Biogeogr 46 (1), 30–44. https://doi.org/10.1111/jbi.13465.

Mann, M.E., Park, J., Bradley, R.S., 1995. Global interdecadal and century-scale climate oscillations during the past five centuries. Nature 378 (6554), 266–270.

Maruyama, F., 2019. Influence of the Atlantic Multidecadal Oscillation and the Pacific Decadal Oscillation on Global Temperature by Wavelet-Based Multifractal Analysis. J. geosci. environ. prot. 07 (08), 105–117. https://doi.org/10.4236/gep.2019.78008.

Melvin, T.M., Briffa, K.R., 2008. A "signal-free" approach to dendroclimatic standardisation. Dendrochronologia 26 (2), 71–86. https://doi.org/10.1016/j.dendro.2007.12.001.

Morrow, P.A., Lamarche, V.C., 1978. Tree ring evidence for chronic insect suppression of productivity in subalpine eucalyptus. Science 201, 1244–1246.

Obojes, N., Meurer, A., Newesely, C., Tasser, E., Oberhuber, W., Mayr, S., Tappeiner, U., 2018. Water stress limits transpiration and growth of European larch up to the lower subalpine belt in an inner-alpine dry valley. New Phytol. 220 (2), 460–475. https://doi.org/10.1111/nph.15348.

Pedregosa, F., Varoquaux, G., Gramfort, A., Michel, V., Thirion, B., Grisel, O., Blondel, M., Müller, A., Nothman, J., Louppe, G., Prettenhofer, P., Weiss, R., Dubourg, V., VanderPlas, J., Passos, A., Cournapeau, D., Brucher, M., Perrot, M., Duchesnay, É., 2011. Scikit-learn: Machine Learning in Python. Journal of Machine Learning Research https://arxiv.org/pdf/1201.0490.

Peek, K., 2018. Sunspot Surprise. Sci. Am. 319 (2), 84. https://doi.org/10.1038/scientificamerican0818-84.

Peters, R.L., Klesse, S., Fonti, P., Frank, D.C., 2017. Contribution of climate vs. larch budmoth outbreaks in regulating biomass accumulation in high-elevation forests. Forest Ecol. Manag. 401, 147–158. https://doi.org/10.1016/j.foreco.2017.06.032.

Pohl, K.A., Hadley, K.S., Arabas, K.B., 2006. Decoupling Tree-Ring Signatures of Climate Variation, Fire, and Insect Outbreaks in Central Oregon. Tree Ring Res. 62 (2), 37–50. https://doi.org/10.3959/1536-1098-62.2.37.

R Development Core Team, 2021. R: A language and environment for statistical computing (Version 4.1.2). R Foundation for Statistical Computing, Vienna, Austria.

Ren, P., Rossi, S., Camarero, J.J., Ellison, A.M., Liang, E., Peñuelas, J., 2018. Critical temperature and precipitation thresholds for the onset of xylogenesis of *Juniperus przewalskii* in a semi-arid area of the north-eastern Tibetan Plateau. Ann. Bot. 121 (4), 617–624. https://doi.org/10.1093/aob/mcx188.

Robock, A., Mao, J., 1995. The Volcanic Signal in Surface Temperature Observations. J. Climate 8 (5), 1086–1103. https://doi.org/10.1175/1520-0442(1995)008<1086:TVSIST>2.0.CO;2.

Rossi, S., Deslauriers, A., Griçar, J., Seo, J.-W., Rathgeber, C.B.K., Anfodillo, T., Morin, H., Levanic, T., Oven, P., Jalkanen, R., 2008. Critical temperatures for xylogenesis in conifers of cold climates. Global Ecol. Biogeogr. 17 (6), 696–707. https://doi.org/10.1111/j.1466-8238.2008.00417.x.

Rowan, A.V., 2017. The 'Little Ice Age' in the Himalaya: A review of glacier advance driven by Northern Hemisphere temperature change. The Holocene 27 (2), 292–308. https://doi.org/10.1177/0959683616658530.

Rozenberg, P., Pâques, L., Huard, F., Roques, A., 2020. Direct and Indirect Analysis of the Elevational Shift of Larch Budmoth Outbreaks Along an Elevation Gradient. Front. For. Glob. Change 3. https://doi.org/10.3389/ffgc.2020.00086.

Ryerson, D.E., Swetnam, T.W., Lynch, A.M., 2003. A tree-ring reconstruction of western spruce budworm outbreaks in the San Juan Mountains, Colorado, U.S.A. Can. J. For. Res. 33 (6), 1010–1028. https://doi.org/10.1139/x03-026.

Shi, F., Fang, K., Xu, C., Guo, Z., Borgaonkar, H.P., 2017. Interannual to centennial variability of the South Asian summer monsoon over the past millennium. Clim. Dyn. 49 (7–8), 2803–2814. https://doi.org/10.1007/s00382-016-3493-9.

Song, M., Zhou, C., Ouyang, H., 2004. Distributions of Dominant Tree Species on the Tibetan Plateau under Current and Future Climate Scenarios. Mt. Res. Dev. 24 (2), 166–173. https://doi.org/10.1659/0276-4741(2004)024[0166:DODTSO]2.0.CO;2.

Speer, J.H., 2010. Fundamentals of Tree-ring Research. University of Arizona Press. https://books.google.de/books?id=XtxEbCzbKUUC.

Thornthwaite, C.W., 1948. An Approach toward a Rational Classification of Climate. Geogr. Rev. 38 (1), 55–94. https://doi.org/10.2307/210739.

Torrence, C., Compo, G.P., 1998. A Practical Guide to Wavelet Analysis. Bull. Amer. Meteor. Soc. 79 (1), 61–78. https://doi.org/10.1175/1520-0477(1998)079<0061:APGTWA>2.0.CO;2.

Virtanen, P., Gommers, R., Oliphant, T.E., Haberland, M., Reddy, T., Cournapeau, D., Burovski, E., Peterson, P., Weckesser, W., Bright, J., van der Walt, S.J., Brett, M., Wilson, J., Millman, K.J., Mayorov, N., Nelson, A.R.J., Jones, E., Kern, R., Larson, E., Carey, C.J., Polat, İ., Feng, Y.u., Moore, E.W., VanderPlas, J., Laxalde, D., Perktold, J., Cimrman, R., Henriksen, I., Quintero, E.A., Harris, C.R., Archibald, A.M., Ribeiro, A.H., Pedregosa, F., van Mulbregt, P., Vijaykumar, A., Bardelli, A.P., Rothberg, A., Hilboll, A., Kloeckner, A., Scopatz, A., Lee, A., Rokem, A., Woods, C.N., Fulton, C., Masson, C., Häggström, C., Fitzgerald, C., Nicholson, D.A., Hagen, D.R., Pasechnik, D.V., Olivetti, E., Martin, E., Wieser, E., Silva, F., Lenders, F., Wilhelm, F., Young, G., Price, G.A., Ingold, G.-L., Allen, G.E., Lee, G.R., Audren, H., Probst, I., Dietrich, J.P., Silterra, J., Webber, J.T., Slavič, J., Nothman, J., Buchner, J., Kulick, J., Schönberger, J.L., de Miranda Cardoso, J.V., Reimer, J., Harrington, J., Rodríguez, J.L.C., Nunez-Iglesias, J., Kuczynski, J., Tritz, K., Thoma, M., Newville, M., Kümmerer, M., Bolingbroke, M., Tartre, M., Pak, M., Smith, N.J., Nowaczyk, N., Shebanov, N., Pavlyk, O., Brodtkorb, P.A., Lee, P., McGibbon, R.T., Feldbauer, R., Lewis, S., Tygier, S., Sievert, S., Vigna, S., Peterson, S., More, S., Pudlik, T., Oshima, T., Pingel, T.J., Robitaille, T.P., Spura, T., Jones, T.R., Cera, T., Leslie, T., Zito, T., Krauss, T., Upadhyay, U., Halchenko, Y.O., Vázquez-Baeza, Y., 2020. SciPy 1.0: fundamental algorithms for scientific computing in Python. Nat Methods 17 (3), 261–272.

Wilson, R., Anchukaitis, K., Briffa, K.R., Büntgen, U., Cook, E., D'Arrigo, R., Davi, N., Esper, J., Frank, D., Gunnarson, B., Hegerl, G., Helama, S., Klesse, S., Krusic, P.J., Linderholm, H.W., Myglan, V., Osborn, T.J., Rydval, M., Schneider, L., Schurer, A., Wiles, G., Zhang, P., Zorita, E., 2016. Last millennium northern hemisphere summer temperatures from tree rings: Part I: The long term context. Quaternary Sci. Rev. 134, 1–18. https://doi.org/10.1016/j.quascirev.2015.12.005.

Wu, Z., Huang, N.E., 2009. Enseble empirical mode decomposition: a noise-assisted data analysis method. Adv. Adapt. Data Anal. 01 (01), 1–41. https://doi.org/10.1142/S1793536909000047.

Wu, X., Mao, J., 2017. Interdecadal variability of early summer monsoon rainfall over South China in association with the Pacific Decadal Oscillation. Int. J. Climatol 37 (2), 706–721. https://doi.org/10.1002/joc.4734.

Xu, X., Miao, Q., Wang, J., Zhang, X., 2003. The water vapor transport model at the regional boundary during the Meiyu period. Adv. Atmos. Sci. 20 (3), 333–342. https://doi.org/10.1007/BF02690791.

Yang, B., Bräuning, A., Liu, J., Davis, M.E., Yajun, S., 2009. Temperature changes on the Tibetan Plateau during the past 600 years inferred from ice cores and tree rings. Glob. Planet. Change 69 (1–2), 71–78. https://doi.org/10.1016/j.gloplacha.2009.07.008.

Zhang, J., Gou, X., Manzanedo, R.D., Zhang, F., Pederson, N., 2018. Cambial phenology and xylogenesis of *Juniperus przewalskii* over a climatic gradient is influenced by both temperature and drought. Agric. For. Meteorol. 260–261, 165–175. https://doi.org/10.1016/j.agrformet.2018.06.011.

Zhang, Y., Li, J., Wang, S., Shao, X., Qin, N., An, W., 2022. A reconstruction of June–July temperature since AD 1383 for Western Sichuan Plateau, China using tree-ring width. Int. J. Climatol. 42 (3), 1803–1817. https://doi.org/10.1002/joc.7336.

Zou, F., Tu, C., Liu, D., Yang, C., Wang, W., Zhang, Z., 2022. Alpine Treeline Dynamics and the Special Exposure Effect in the Hengduan Mountains. Front. Plant Sci. 13, 1–14. https://doi.org/10.3389/fpls.2022.861231.